Journal of Power Sources 184 (2008) 220–228

Contents lists available at ScienceDirect

Journal of Power Sources

journal homepage: www.elsevier.com/locate/jpowsour

The effect of surface treatment on the oxidation of ferritic stainless steels used for solid oxide fuel cell interconnects

L. Cooper [a], S. Benhaddad [b], A. Wood [b], D.G. Ivey [a,*]

[a] Department of Chemical and Materials Engineering, University of Alberta, Edmonton, Alberta, Canada T6G 2G6
[b] Versa Power Systems, Calgary, Alberta, Canada T2B 3R2

ARTICLE INFO

Article history:
Received 30 April 2008
Received in revised form 2 June 2008
Accepted 4 June 2008
Available online 14 June 2008

Keywords:
Interconnects
Solid oxide fuel cells
Ferritic stainless steels
Surface treatment
Oxidation

ABSTRACT

Ferritic stainless steels are candidate interconnect materials for solid oxide fuel cells (SOFC); however, the oxidation resistance of commercial stainless steels within the operating temperature range of 700–800 °C is not adequate. A relatively thick, poorly conducting oxide layer forms on the surface of the stainless steel interconnect, decreasing cell performance. One way of modifying the oxidation behaviour of an alloy is through surface treatment. The aim of this work is to perform a systematic study of the effect of surface treatment (sandblasting and cold rolling) on the oxidation behaviour of three different ferritic stainless steels at 800 °C in air. Oxidized specimens are characterized using X-ray diffraction (XRD) and scanning electron microscopy (SEM). In addition, specimens oxidized under the same conditions for 15 min are examined using secondary ion mass spectrometry (SIMS) depth profiling and X-ray photoelectron spectroscopy (XPS) depth profiling.

For all three steels, the as-is (undeformed) specimens have a lower mass gain than the deformed specimens. The steel with the highest Cr content has significantly higher mass gains than the other two steels, which have similar mass gains. X-ray diffraction and electron microscopy results indicate that the oxide scale formed on all the specimens consists of an inner layer of chromia and an outer spinel layer. The relative amounts of the two oxide phases present depends on both the steel and treatment condition. The presence of insulating oxides at the metal/oxide interface is detected with both surface science techniques and electron microscopy.

1. Introduction

Intermediate temperature solid oxide fuel cells (SOFCs) typically operate in the temperature range of 700–800 °C. A single cell consists of an anode and cathode separated by a solid, oxygen-ion conducting electrolyte. In order to obtain output voltages sufficient for practical applications, single cells are electrically connected in series by interconnects to form a fuel cell stack. A suitable interconnect material must satisfy many requirements under SOFC operating conditions, including the following: high electrical conductivity, high thermal conductivity, sufficient high temperature mechanical strength and creep resistance, thermal expansion coefficient compatibility with the other stack components and chemical stability [1,2]. However, in order for SOFC commercialization to be possible, the interconnect must also be inexpensive and relatively easy to fabricate. Although ceramic interconnects have a higher resistance to oxidation, metallic interconnects are more ductile, less expensive and significantly easier to manufacture. Ferritic stainless steels containing 16–26 wt% Cr are particularly promising due to their low cost, machinability and thermal expansion coefficient compatibility with other stack materials. The main problem with the use of ferritic stainless steels as interconnect materials is their inadequate high temperature oxidation resistance. Under SOFC operating conditions, ferritic stainless steels form a poorly conductive oxide layer which increases the electrical resistance of the interconnect, resulting in a decrease in fuel cell performance. In addition, the oxide scale is susceptible to spalling during normal fuel cell operation, in particular during thermal cycling encountered at start-up and shutdown.

One way of modifying the oxidation behaviour of an alloy is through the use of a surface treatment such as polishing, electropolishing, grinding, shot peening, sandblasting, machining or cold rolling. The effect of surface treatment on oxidation has been described previously in the literature. As a result of surface treatment, energy is stored in the surface region of a metal in the form of dislocations [3,4]. Initially, these dislocations act as fast diffusion paths, increasing the rate of transport of protective scale-forming elements to the metal surface. Assuming that the oxidation tem-

* Corresponding author. Tel.: +1 780 492 2957; fax: +1 780 492 2881.
E-mail address: doug.ivey@ualberta.ca (D.G. Ivey).

0378-7753/$ – see front matter © 2008 Elsevier B.V. All rights reserved.
doi:10.1016/j.jpowsour.2008.06.010

perature is higher than the recrystallization temperature, recovery and recrystallization then occur, resulting in the formation of a fine-grained surface microstructure. In the later stages of oxidation, following the annihilation of dislocations by recovery and recrystallization, it is these grain boundaries and subgrain boundaries that act as fast diffusion paths for scale-forming elements [3–6]. Therefore, preferential oxidation of the scale-forming elements can result in easier formation of a protective oxide layer for a surface treated metal. Also, the increased transport of scale-forming elements from the bulk of the metal results in reduced depletion of scale-forming elements in the region directly below the metal/oxide interface.

The purpose of this study was to examine the effect of two different surface treatments, sandblasting and cold rolling, on the oxidation behaviour of several ferritic stainless steels. A number of different characterization techniques, including scanning electron microscopy (SEM), energy-dispersive X-ray analysis (EDX), X-ray diffraction (XRD), X-ray photoelectron spectroscopy (XPS) and secondary ion mass spectrometry (SIMS), were used to analyze the oxide layers that formed on the ferritic stainless steels at 800 °C in air after both short-term and long-term exposure.

2. Experimental methods

Three ferritic stainless steels were selected for this study, hereafter referred to as SS1, SS2 and SS3. The compositions of the three steels are listed in Table 1. SS1 has the same composition as an AISI-SAE 430 stainless steel, SS2 has slightly more Cr than SS1, as well as small amounts of Nb and Mo, and SS3 has the highest amount of Cr (22 wt%) with additions of Ni, Al, La and Zr. For each steel, specimens approximately 2.5 cm × 2.0 cm in size were cut from sheets that had been cold rolled and bright annealed before any subsequent mechanical processing. The thickness of SS1 and SS2 specimens was approximately 1 mm, while the thickness of the SS3 specimens was approximately 0.25 mm.

Two different surface treatment methods were used in this study: sandblasting and cold rolling. Sandblasting was done on only one side of the steel and was performed on the sheet metal before it was cut into specimens. Alumina particles (100 grit) were used in the sandblasting process. The particles were projected towards the steel surface under 0.7 MPa pressure using a nozzle with an inside diameter of 2.3 cm that was held 8–10 cm above the steel sheet. Samples were subjected to either 1 pass or 10 passes, with each pass taking 3 s to cover a steel strip that was 13 cm in length and 2.5 cm in width. Cold rolling was carried out using a rolling mill and was performed on the individual specimens after cutting. The rolling direction was parallel to the length of the specimens. Two different thickness reductions were studied: 6% and 15% for the SS1 and SS2 specimens, and 8% and 21% for the SS3 specimens.

Prior to oxidation, the specimens were cleaned with soap and rinsed with deionized water followed by ethanol. For the long-term oxidation experiments, the specimens were weighed to the nearest 0.01 mg using a high precision balance and then placed in alumina crucibles, which were then put in a box furnace. Oxidation was carried out at 800 °C in air. Specimens were removed from the furnace at regular intervals, for times up to 502 h. Following removal from the furnace, the specimens were cooled to room temperature and then weighed. For the short-term oxidation experiments, a similar procedure was followed except the specimens were not weighed and the oxidation time was 15 min.

XRD analysis of the oxidized specimens was carried out with a Rigaku Geigerflex 2173 system with a vertical goniometer. The X-ray source was Co, with Kα X-rays having a wavelength of 0.179021 nm. Analysis of the data was carried out using Jade software.

Cross section specimens, for microstructural analysis, required careful preparation. First, a thin layer of Au (~12 nm thick) was sputter coated on both sides of the oxidized specimens. Then, a layer of Ni was electrodeposited using a Watts Ni solution at a temperature of 40–60 °C at a current density of 60 mA cm^{-2} for 30 min. The purpose of the Ni layer was to protect the oxide layer from cracking and spalling during grinding and polishing. The specimens were then cold mounted, ground and polished using standard metallographic techniques, finishing with 0.05 μm alumina slurry. SEM analysis of cross section specimens was carried out using a Hitachi S-2700 SEM with a Princeton Gamma Tech (PGT) PRISM IG (intrinsic germainium) detector for energy-dispersive X-ray analysis. The imaging and EDX collection were performed using PGT IMIX software.

Secondary ion mass spectrometry depth profiling was used to determine the distribution of various elements in the oxide layers formed on the steel specimens oxidized for 15 min, as well as in the native oxide. SIMS analysis was carried out using an ION-ToF SIMS IV. Sputtering was done with Cs^+ ions at 1 keV and 250 nA over an area 200 μm × 200 μm. For analysis, Ga^+ ions at 15 keV and an area of 34 μm × 34 μm were used, corresponding to 128 × 128 pixels.

X-ray photoelectron spectroscopy (XPS) depth profiling was used to determine the chemical state of various elements in the oxide layers formed on as-is and cold rolled steel specimens oxidized for 15 min, as well as in the native oxide. A Kratos Axis 165 XPS system was utilized, with a monochromatic Al X-ray beam with a Kα energy of 1486.6 eV. Sputtering was carried out with Ar^+ ions with an accelerating voltage of 4 kV. Analysis of the XPS results was carried out using Casa software.

Table 1
Composition of ferritic stainless steels [7,8]

Composition (wt%)	Steel		
	SS1	SS2	SS3
C	0.12 max	0.12 max	0.02
Cr	16–18	19	22
Fe	Balance	Balance	Balance
Mn	1 max	1 max	0.5
P	0.04 max	0.04 max	–
Si	1 max	1 max	0.4
S	0.03 max	0.03 max	–
Mo	–	2	–
Nb	–	0.35	–
Ni	–	–	0.26
Al	–	–	0.22
La	–	–	0.04
Zr	–	–	0.22

3. Results

3.1. Specific mass gain

The specific mass gain results have been reported previously, so are only summarized here (Table 2) [9]. The oxidation of all specimens was found to follow parabolic kinetics. In general, the

Table 2
Parabolic rate constants (×10^{-14} g^2 cm^{-4} s^{-1})

Surface treatment	SS1	SS2	SS3
As-is	5.62	3.87	20.5
As-is (thin)	12.8	3.20	–
Rolled–6% (8% SS3)	5.60	4.73	25.7
Rolled–15% (21% SS3)	6.85	6.18	28.3
Sand blasted–1 pass	12.0	4.76	24.0
Sand blasted–10 passes	6.34	3.35	24.5

specific mass gain of the treated specimens was larger than for the as-is specimens. In addition, the parabolic rate constants for the SS3 specimens were a factor of 2–3 larger than for the other two steels. The parabolic rate constants for the SS1 and SS2 specimens were similar, with those for SS2 being slightly lower.

3.2. X-ray diffraction

X-ray diffraction was carried out on specimens oxidized for 50 h and 502 h in order to determine the oxide phases present. The results of this analysis have been reported elsewhere [9], so again only a summary of the results is presented here. For all three steels, two oxide phases were identified: Cr_2O_3 and $(Cr,Mn)_3O_4$ spinel. The relative amount of spinel present in the oxide scale differed depending on the steel and treatment condition. SS3 had the highest relative amount of spinel, followed by SS1, and then SS2. For SS3 and SS1, the as-is specimen had relatively more spinel than the treated specimens, while for SS2, all the specimens had a similar relative amount of spinel.

3.3. SEM analysis

Fig. 1(a) shows an SEM SE image of the SS3 as-is specimen oxidized for 502 h. The EDX spectra taken from the inner and outer regions of the oxide scale are shown in Fig. 1(b and c), respectively. Fig. 1 indicates that the chromia formed a continuous layer adjacent to the steel, while Cr–Mn spinel particles were located in the outer region of the oxide scale. The oxide scales that formed on the oxidized specimens of the other steels and treatment conditions all had a morphology similar to that shown in Fig. 1.

In order to investigate the differences between the oxide scales of the three steels, EDX linescans were carried out on the cross section specimens oxidized for 502 h and are shown in Fig. 2. In Fig. 2(a), the linescan shows that for SS1, Fe was present in the steel but depleted in the oxide layer. Chromium was present in the steel and enriched in the oxide layer, with the amount of Cr in the inner oxide higher than that in the outer oxide. Manganese was present mainly in the outer oxide. Silicon had segregated to the metal/oxide interface, likely forming a thin layer of SiO_2. Fig. 2(b) reveals that for SS2, the Fe, Cr, and Mn distributions in the oxide scale were similar to SS1. Silicon segregation to the metal/oxide interface was not clearly evident for SS2. The Mo and Nb profiles from Fig. 2(b) indicate that they are present as carbides in the steel; however, they did not appear to be present in the oxide scale. Fig. 2(c) indicates that the Fe, Cr, and Mn distributions for SS3 were the same as for SS1 and SS2. For SS3, Si segregation to the metal/oxide interface was evident; Al segregation was similarly observed. Neither Zr nor La was detected in the oxide scale.

Fig. 2 displays the linescans for the oxidized untreated specimens only; however, the element distribution did not differ significantly for either the rolled or sandblasted specimens, so the profiles are not shown here. The oxide scales on the sandblasted specimens, however, were significantly less uniform in thickness than for the as-is specimens.

3.4. Surface analysis

In order to investigate the early stages of oxide formation, SIMS and XPS analysis and depth profiling were carried out on specimens that were oxidized for 15 min at 800 °C. The SIMS depth profiles for the SS1 as-is specimen are shown in Fig. 3. In Fig. 3, sputtering time increases along the horizontal axis, corresponding to increasing depth through the oxide scale. Iron was depleted in the oxide layer relative to the amount present in the bulk of the steel, and Cr was enriched throughout the oxide scale. Manganese segregation to the surface of the oxide was observed, with the amount of Mn present decreasing throughout the oxide layer and into the bulk of the steel. Silicon was also present at the surface of the oxide but the majority of the Si was segregated to the metal/oxide interface. Similar profiles were obtained for the rolled and sandblasted specimens and for SS2 and SS3.

In order to determine the chemical state of the elements present in the oxide scale, i.e., whether they were present in the metallic or oxide form, XPS analysis was carried out. Fig. 4 shows Cr, Fe, Mn and Si spectra for SS1 taken at different sputtering intervals. From Fig. 4(a), it can be seen that all the Cr at the surface of the oxide was in the oxide form. The Cr oxide peak remained as sputtering continued through the oxide layer. Then, a small Cr metal peak was

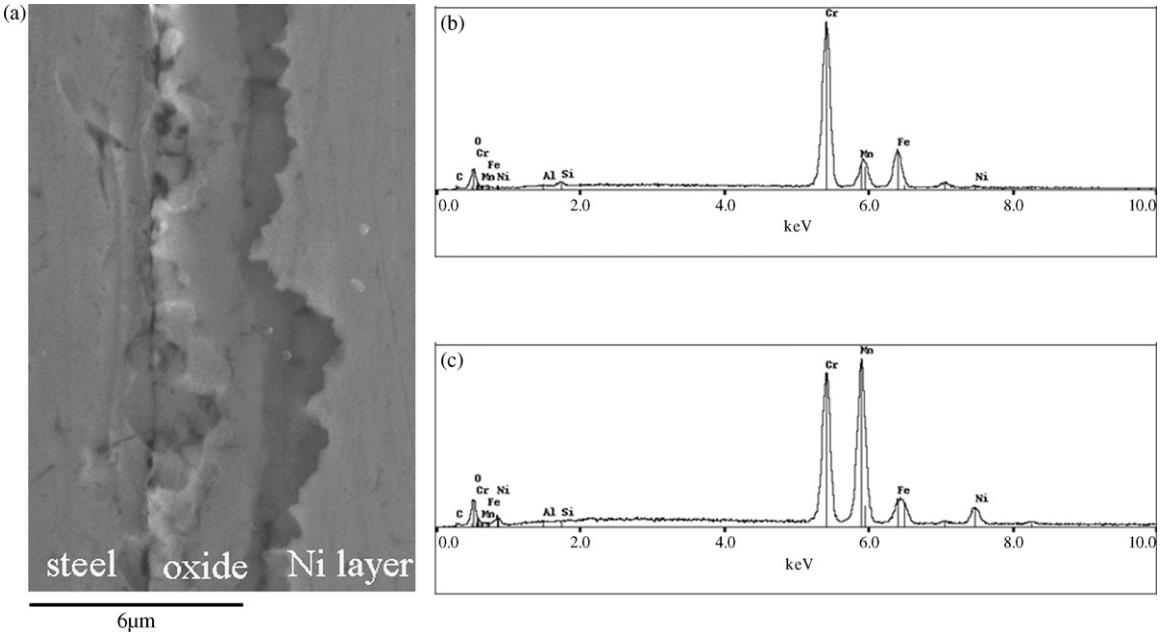

Fig. 1. SS3 specimen oxidized for 502 h: (a) SEM SE image; (b) EDX spectrum from inner chromia; (c) EDX spectrum from outer spinel.

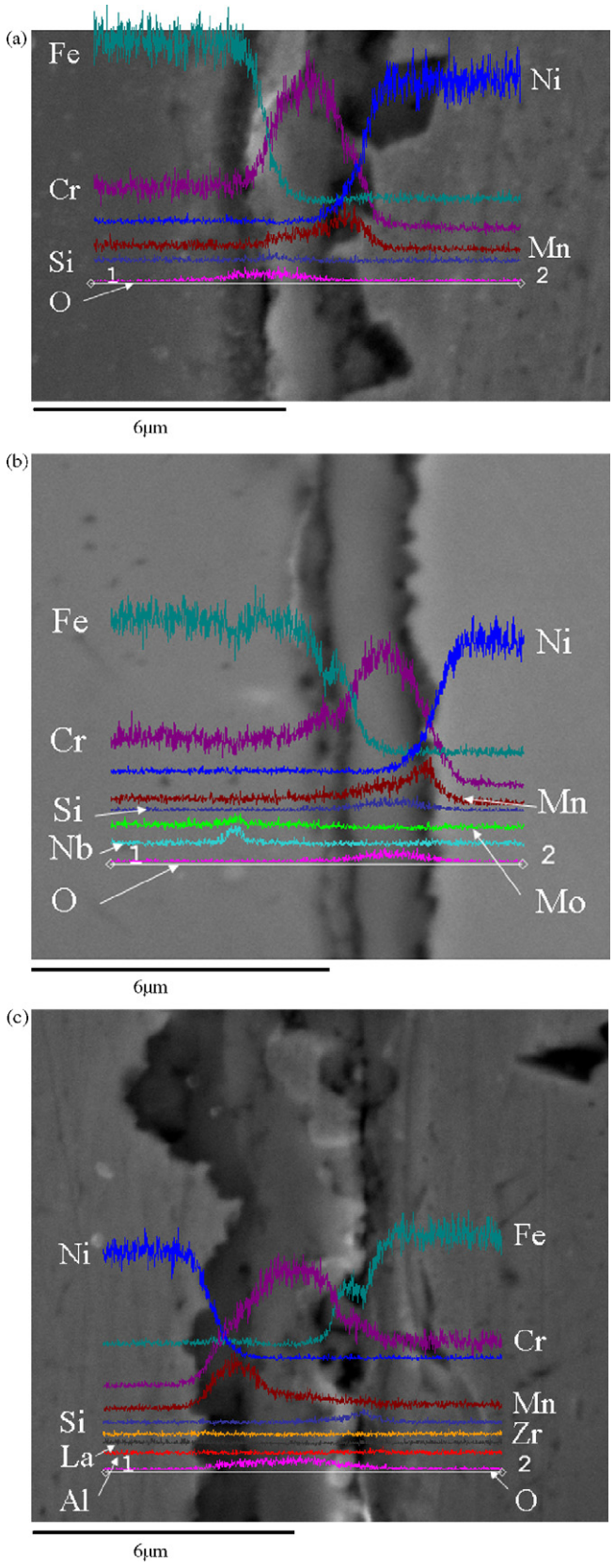

Fig. 2. EDX linescans of cross section specimens oxidized for 502 h: (a) SS1 as-is; (b) SS2 as-is; (c) SS3 as-is.

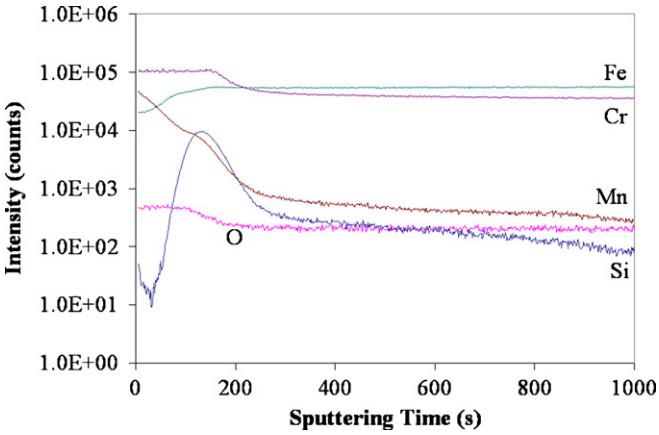

Fig. 3. SIMS depth profile of SS1 as-is specimen oxidized for 15 min at 800 °C.

detected after 3960 s. The oxide peak decreased in height and the metallic peak became stronger with further sputtering, indicating the steel substrate was reached. Fig. 4(b) shows that, initially, a Fe oxide peak was present indicating that some Fe in oxide form was incorporated in the oxide scale. This peak remained upon sputtering and, after some time, a Fe metal peak also appeared. Then, the oxide peak disappeared and the metal peak became larger. By comparing Fig. 4(a and b), it is apparent that the transition of Fe from the oxidized state to the metallic form occurred sooner than for Cr. This is most likely a sputtering artifact resulting from sputtering being carried out at a 45° angle to the specimen surface. If the Fe peaks in Fig. 4(b) are compared with the Si peaks in Fig. 4(d), the Fe oxide peak is present up to and including a sputtering time of 3960 s. In addition, the Si oxide peak indicating the metal/oxide interface appears at a sputtering time of 4560 s. This suggests that the Fe in the oxide scale is in the oxidized form, and the Fe in the bulk of the steel is in the metallic form. Fig. 4(c) indicates that Mn was present in its oxidized form throughout the oxide; however, the peaks are stronger in the outer region of the oxide scale, indicating that the Mn was segregated to the outer portion of the oxide scale. Manganese was not present in metallic form below the oxide layer, suggesting either a depleted zone or simply that the amount present was small. The steels nominally contain about 1 wt% Mn. For Si, the spectra were noisy; however, there was a small oxide peak present prior to sputtering, indicating the presence of oxidized Si at the surface of the oxide layer. Fig. 4(d) also shows a Si oxide peak after 4560 s of sputtering, indicating that SiO_2 had formed at the metal/oxide interface.

SIMS depth profiles for SS2 are shown in Fig. 5. In comparing Fig. 5 with the SS1 depth profiles in Fig. 3, it can be seen that the Fe, Cr, and Mn distributions are similar for the two steels. For SS2, both Si and Nb are segregated to the metal/oxide interface, while Mo is depleted in the oxide scale compared to its level in the bulk of the steel.

XPS analysis was also carried out on the SS2 specimens. The Cr, Fe and Mn peaks followed a similar trend as that found for SS1. For Si, although the SIMS analysis indicated that Si segregation to the metal/oxide interface was present, no Si XPS peaks were clearly present and the Si signal was quite noisy. The plots for Mo and Nb are shown in Fig. 6. For Mo, no peaks were present during the initial sputtering. Molybdenum metal peaks appeared in Fig. 6(a) only after very long sputtering times, indicating that Mo was not present in the oxide scale but remained in the steel substrate. Fig. 6(b) indicates that on the surface of the oxide layer, Nb was present in the oxidized form. The Nb oxide peak is situated between the NbO_2 and NbO_5 peak positions, indicating that the Nb has a charge between +4 and +5. It is likely that either a mixture of

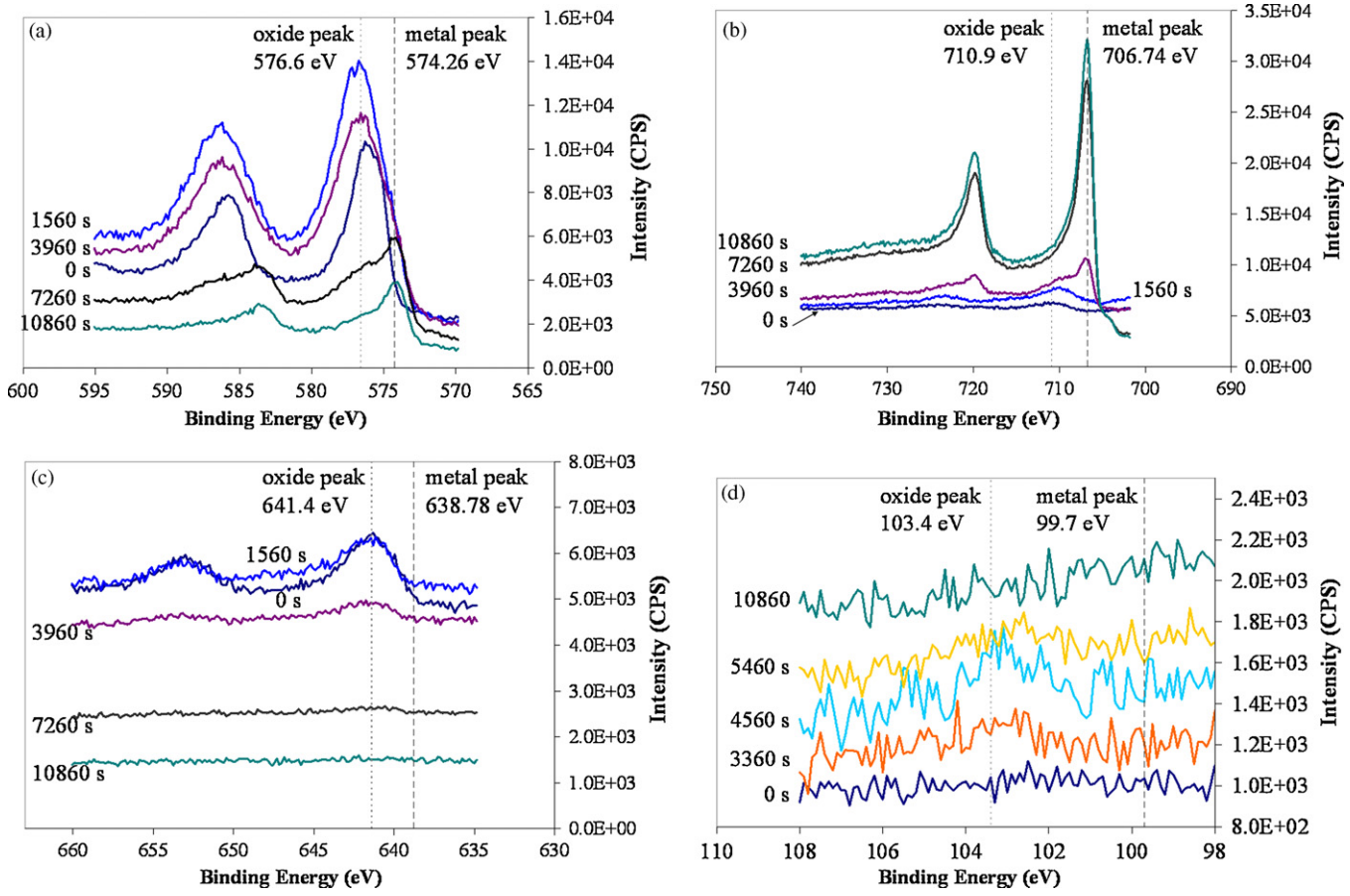

Fig. 4. XPS 2p peak plots for SS1 as-is specimen oxidized for 15 min at 800 °C: (a) Cr; (b) Fe; (c) Mn; (d) Si.

the two oxides is present, or that Nb has been incorporated into a mixed oxide. Although the Nb signal is quite noisy, Nb appears to be present in the oxide form at the metal/oxide interface, which confirms the SIMS results. After long sputtering times, the Nb metallic peak appeared, indicating the presence of Nb in the steel.

Fig. 7 shows SIMS depth profiles for the SS3 specimen. The Cr, Fe, Mn and Si distributions for SS3 were similar to those previously described for SS1 and SS2. The distribution of Al was similar to that for Si. Neither Zr nor Ni appeared to be present in the oxide scale. Lanthanum was enriched in the oxide scale compared with the amount present in the bulk of the steel, although it was difficult to identify exactly where in the oxide scale the La was located as the signal for La was quite noisy.

XPS analysis for SS3 revealed that the Cr, Fe and Mn peak profiles were similar to those for SS1 and SS2. The Si and Al peak profiles are shown in Fig. 8. Fig. 8 indicates that both Si and Al oxide peaks are present at the metal/oxide interface, corresponding with the segregation seen in the SIMS depth profile in Fig. 7.

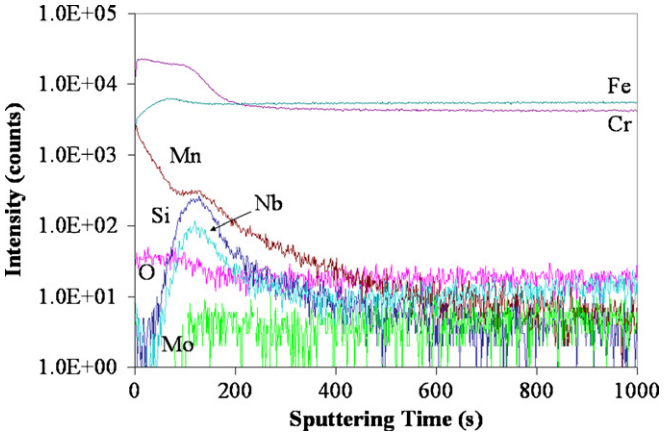

Fig. 5. SIMS depth profile of SS2 as-is specimen oxidized for 15 min at 800 °C.

4. Discussion

4.1. Specific mass gain

For SOFC interconnect applications, it is important to reduce the overall scale thickness that forms on the interconnect during fuel cell operation. This is because thick scales result in interconnect dimensional changes which can reduce the load bearing ability of the interconnect [10]. Also, thick oxide scales can block air and fuel channels, reducing fuel cell performance [10]. Therefore, it is important that specific mass gain due to oxidation be as low as possible. In long-term oxidation experiments carried out under simulated SOFC cathode operating conditions (air and 800 °C), it was found that the specific mass gain for SS3 was significantly higher (by a factor of approximately 2–3) than that for both SS1 and SS2 [9]. The SS1 and SS2 steels had similar specific mass gains with those for SS2 being slightly smaller.

One reason for the difference in specific mass gain between the three steels is the amount of Cr available for oxide formation. The SS1 steel nominally contains 16–18% Cr, while SS2 contains 19% Cr

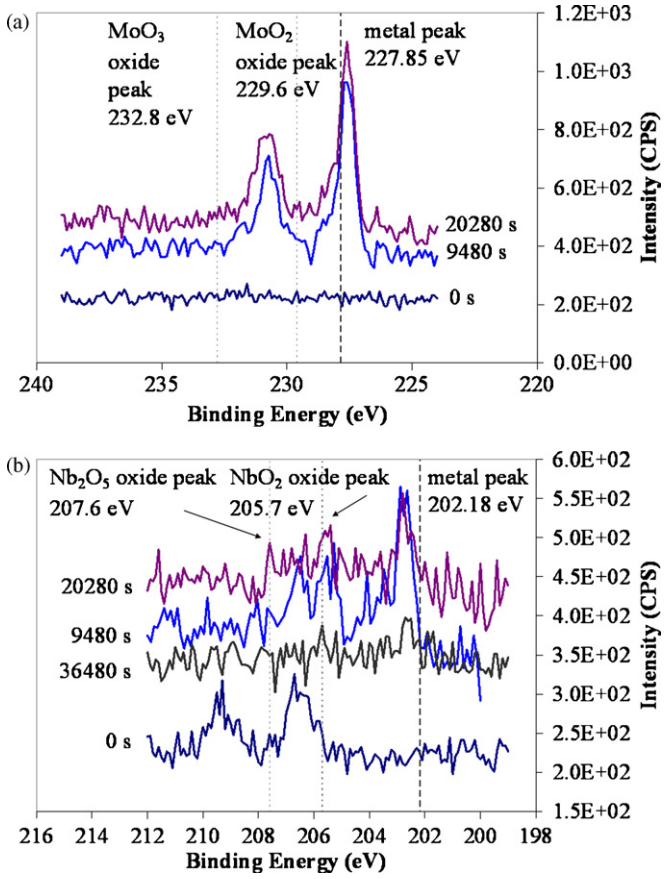

Fig. 6. XPS peak plots for SS2 as-is specimen oxidized for 15 min at 800 °C: (a) Mo; (b) Nb.

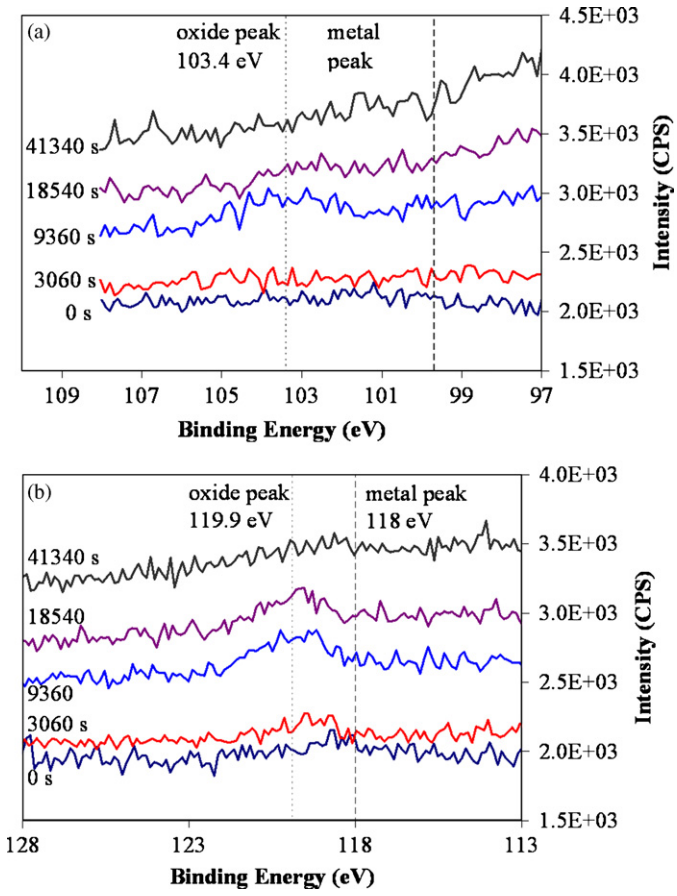

Fig. 8. XPS 2p peak profiles for SS3 as-is specimen oxidized for 15 min at 800 °C: (a) Si; (b) Al.

and SS3 contains 22% Cr. In addition, SS2 and SS3 contain carbide-forming elements, allowing more Cr to be available for protective oxide formation. The SS1 steel does not contain additional carbide formers, so that the amount of Cr available for oxidation is reduced due to the formation of Cr carbides. First of all, it is important to determine whether or not enough carbide-forming elements are added to SS2 and SS3 to tie up all the C. For SS2, both Nb and Mo are added. An approximate calculation of the amount of Cr available for oxide formation can be carried out by assuming that no Cr or Fe is involved in carbide formation, all the Nb forms NbC and the Mo forms Mo_2C [11]. The formation of Nb and Mo carbides in

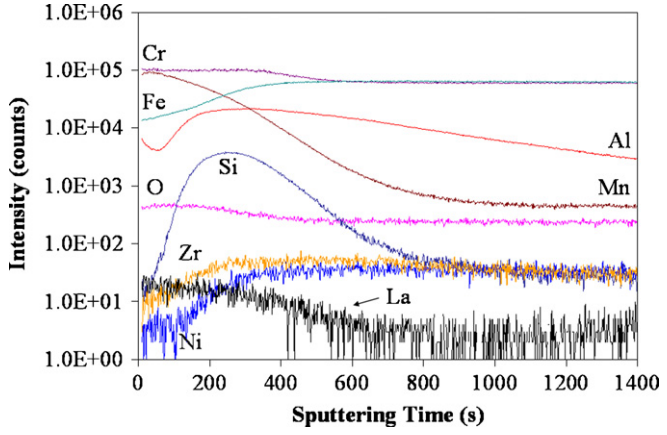

Fig. 7. SIMS depth profile of SS3 as-is specimen oxidized for 15 min at 800 °C.

SS2 was confirmed through EDX analysis and electron diffraction in the transmission electron microscope (TEM), although the results are not presented here. Since Nb is the strongest carbide-forming element, it is assumed that all the Nb will form NbC. This leaves 0.073 wt% C available for carbide formation with Mo. Assuming that Mo_2C forms, 1.17 wt% Mo is used to tie up the remaining C, leaving 0.83 wt% Mo in the bulk of the steel. This means that based on the amount of carbide formers added, all the C could be tied up in Nb and Mo carbides, leaving all the Cr in SS2 available for oxide formation. For SS3, Zr is added to form ZrC. The presence of ZrC was again confirmed by TEM analysis. From the steel composition, enough Zr is present so that all the C will form ZrC, leaving 0.07 wt% Zr in the bulk of the steel. In order to determine the amount of Cr available for oxide formation in SS1, the amount of Cr tied up in carbide formation must be calculated. Assuming that all the C forms $Cr_{23}C_6$ [12], 2.0 wt% Cr is used up in carbide formation. This leaves 14.0 wt% Cr available for oxide formation in SS1. Therefore, as a best case estimate, SS2 and SS3 have up to 5 wt% more Cr and 8 wt% more Cr, respectively, available for protective scale formation than SS1. According to the above estimates, since no significant spalling was found on any of the specimens, it would seem that the higher specific mass gain for the SS3 specimens can be correlated with the fact that this steel has more Cr available for protective oxide formation than either SS1 or SS2. However, since SS2 has more Cr available for oxide formation than SS1, it would be expected that the specific mass gain for the SS2 specimens would be higher than for the SS1 specimens, which was not the case. It has been reported in the literature that the minimum amount of Cr required for protective scale formation is reduced as alloy grain size is reduced because of the

increase in the grain boundary density, which allows for more rapid transport of scale-forming elements to the surface of the alloy [13]. Upon examination of etched cross section specimens in the SEM, the grain size of the SS2 steel was approximately twice as large as for the other two steels prior to oxidation. The grain size of the SS1 and SS3 specimens was similar, in the range of 10–20 μm, while the grain size for SS2 was 25–35 μm. The resulting reduced rate of Cr transport to the surface for SS2 could explain why the specific mass gain for SS2 was lower than that for SS1, despite SS2 having more Cr available for protective oxide formation.

In general, the specific mass gain for the treated specimens was higher than for the as-is specimens. It appears that under the oxidation conditions studied (air and 800 °C), the increased rate of transport of scale-forming elements (Cr, Mn, Si, Al, etc.), by way of fast diffusion paths such as dislocations, grain boundaries, and subgrain boundaries, to the metal/oxide interface has resulted in an increase in the overall oxidation rate of the three steels.

For all three steels, a higher specific mass gain corresponded to specimens that had undergone a higher rolling reduction, which could be related to the depth of the deformed region. This would mean that the recrystallized region would extend deeper into the metal, allowing for faster transport of scale-forming elements to the surface. Also, an increase in the amount of deformation would mean an increase in the number of dislocations in the surface region of the metal, producing a finer surface microstructure following recrystallization. In the literature, several studies have been done on the effect of the degree of cold rolling on oxidation behaviour. In a study of the oxidation of Inconel 625 (58Ni–1Co–21.5Cr–9Mo–5Fe—compositions are in wt%) in air at 1000 °C for up to 36 h, the mass gain due to oxidation decreased as the cold rolling reduction was increased from 10% to 30% [14]. A study of the oxidation of Incoloy 800 in superheated steam at 600 °C for 1000 h also found that the weight gain due to oxidation decreased as the amount of cold work increased from 10% to 90% [15]. The latter study also found that the oxidation kinetics changed from parabolic to cubic to logarithmic as the rolling reduction was increased [15]. In the current study, the amount of rolling reduction did not change the oxidation kinetics. It is not clear why the current study showed an opposite trend to the two other studies in the literature (an increase instead of a decrease in the mass gain due to oxidation with an increase in the cold rolling reduction). The difference in material or oxidation conditions may account for the discrepancy.

In general, the sandblasted specimens in this study had a higher mass gain than the as-is specimens. Several studies have also reported an increase in the mass gain due to oxidation following a sandblasting treatment. One study of several stainless steels containing between 9 and 20 wt% Cr at 600 °C for 100 h, in both air and reducing environments, found that the oxide scale thickness was larger for sandblasted specimens than for electropolished, polished, or ground specimens [3]. Similar results were reported in a study of 9 wt% Cr steels containing Mo and 12 wt% Cr steels, containing Mo and V, in air and reducing environments at 600 °C for 100 h [16]. However, a study of an iron-based oxide dispersion strengthened (ODS) FeCrAl alloy, annealed at 1000 °C for up to 100 h, found that the oxide scale thickness formed on specimens that were sandblasted with alumina for 30 min was smaller than that on specimens that were polished with 1 μm alumina paste [17]. The increase in surface roughness produced by the sandblasting treatment would be expected to result in an increased oxide nucleation rate, not only because of the increased surface area of the rougher surface, but also because the sandblasted surface has more sharp edges and points which act as preferred nucleation sites [18]. In this study, the difference in surface area between the sandblasted specimens and the other specimens was not found to be significant; however, SEM analysis of the sandblasted specimens prior to oxidation confirmed the presence of sharp edges and points.

Table 3
Chromia thickness comparison

Steel	Chromia thickness (μm)
SS1	1.00 ± 0.20
SS2	1.32 ± 0.19
SS3	2.71 ± 0.30

One criterion of a surface treatment is that it should uniformly deform the surface of a material so that an oxide scale of uniform thickness is produced [19,20]. For the sandblasted specimens, cross sections of the oxide layer revealed that this was not the case; the oxide thickness was found to vary significantly along the specimen surface. It is also important that a surface treatment does not introduce contaminant species to the surface of the alloy as this can result in an increase in the oxidation rate of the alloy [21]. The impurities could either act as nucleation sites for oxide formation, or could themselves oxidize. For the SS1 and SS2 rolled specimens, rapidly growing clumps of oxide enriched with impurities (Ni, Sn, Cu, P, Si, and Al) were detected after 502 h of oxidation. These impurities may have been introduced during the rolling treatment and acted as nucleation sites for oxide formation. For the sandblasted specimens, alumina particles containing a small amount of Ti were found to be imbedded in the surface of the steel prior to oxidation. These particles may have acted as preferred nucleation sites for oxide formation. It is unlikely that a cleaning process such as ultrasonic cleaning would be able to remove the alumina particles from the stainless steel substrate.

From the specific mass gain results, it was determined that for all specimens, the parabolic oxidation model was the best fit for the measured data. The parabolic oxidation model assumes that the oxidation process is diffusion limited, meaning that the rate of oxidation is limited by the rate of diffusion of either oxygen or metal ions across the oxide scale [22]. This result is not surprising as parabolic oxidation is known to describe the oxidation of most metals at high temperatures [22]. In this study, the parabolic rate constants were found to vary between 5 and 13×10^{-14} g^2 cm^{-4} s^{-1} for the SS1 specimens, between 3 and 7×10^{-14} g^2 cm^{-4} s^{-1} for the SS2 specimens, and between 20 and 29×10^{-14} g^2 cm^{-4} s^{-1} for the SS3 specimens (Table 2) [9]. In order for ferritic stainless steels to be suitable for SOFC interconnect applications, a parabolic rate constant below 10^{-14} g^2 cm^{-4} s^{-1} is required, and a value below 10^{-15} g^2 cm^{-4} s^{-1} would be ideal [23]. This value is based on a calculation of the oxide layer thickness at the target SOFC lifetime of 40,000 h assuming fully dense chromia forms [24]. As none of the steels or treatment conditions resulted in a parabolic rate constant within the required range, further modifications are required in order for the steels tested to be suitable for SOFC interconnect applications.

4.2. Spinel

For all three steels, the relative amount of spinel compared to chromia in the oxide scale increased with increasing oxidation time [9]. In addition, the SS3 specimens had the highest relative amount of spinel, followed by the SS1 specimens, and then the SS2 specimens. Steels with more Mn tend to form more spinel than steels of a similar composition with less Mn [25]. According to the steel specifications (Table 1), SS3 has 0.5 wt% Mn while SS1 and SS2 contain a maximum of 1 wt%. Therefore, it is unlikely that there is more Mn present in SS3 than in the other two steels.

Table 3 displays the average chromia thickness determined from cross section SEM images. The chromia thickness for SS3 was much

Table 4
Comparison of spinel phase composition

Surface treatment	SS1		SS2		SS3*	
	Cr:Mn	Cr:Fe	Cr:Mn	Cr:Fe	Cr:Mn	Cr:Fe
As-is	2.3	13.3	1.9	4.4	0.8	4.6
Rolled 6% (*8%)	2.3	16.5	2.4	13.1	1.5	6.4
Rolled 15% (*21%)	1.7	10.9	3.9	18.6	0.8	3.7
Sandblasted 1 pass	1.7	7.6	1.9	10.5	1.2	4.9
Sandblasted 10 passes	1.8	10.3	1.9	6.4	1.2	5.4

* Indicates that this steel is rolled 8% and 21%, as indicated in the first column.

larger than that for the other two steels (by a factor between 2 and 3). The chromia thickness for SS2 was larger than for SS1. A thinner layer of chromia would result in a reduced diffusion distance for Mn to travel from the metal/oxide interface to the outer region of the oxide scale, leading to an increase in the relative amount of spinel present. However, SS3 had the thickest chromia layer and the thickest spinel layer for a given surface treatment. The chromia that formed on the SS3 specimens may have been less protective than for the SS1 or SS2 specimens, permitting more rapid diffusion of Mn through the chromia layer. The reason for the chromia being less protective for SS3 is not clear at this time, especially since SS3 contains La, which is supposed to improve the protective ability of the chromia. The formation of a thicker chromia layer for SS2 is most likely due to the increased amount of Cr available for oxide formation compared with SS1. The thicker chromia layer for SS2 could account for the lower amount of spinel relative to SS1.

For SS1 and SS3, surface treatment was found to have an effect on the relative amount of spinel that formed. Relatively more spinel compared to chromia formed on the as-is specimens in comparison to the treated specimens. The treated samples also had thicker chromia layers, which would reduce the Mn diffusion flux through the chromia resulting in less spinel formation. It appears that the effect of surface treatment on the supply of Cr from the bulk and subsequent chromia formation is more significant than the increased supply of Mn from the bulk. For SS2, a similar amount of spinel formed on all specimens.

The relative amounts of spinel and chromia in the oxide scale are significant for SOFC interconnect applications. The resistance of the oxide scale is proportional to its thickness; therefore, interconnects should not form thick oxide scales [10,20]. The conductivity of the spinel phase is considered to be higher than that of chromia. However, the values reported in the literature for the resistivity of chromia and various Cr–Mn spinels vary significantly. For Cr_2O_3, the resistivity has been reported as $1.8 \times 10^4\ \Omega$ cm [26] and 200 Ω cm [27] at 750 °C. For $MnCr_2O_4$, the resistivity at 750 °C has been measured as 7.2 Ω cm [26] and as 1900 Ω cm at 800 °C [28]. As the relative amount of Mn in the spinel increases, the resistivity decreases. For $Mn_{1.5}Cr_{1.5}O_4$, the resistivity at 750 °C is 4 Ω cm [26]. For Mn_2CrO_4, the resistivity at 800 °C is 3.5 Ω cm [28]. Because of the large difference in the conductivity of the chromia and spinel phases, the overall conductivity of a thicker oxide scale containing a large relative amount of spinel may in fact be higher than that of a thinner oxide scale consisting mainly of chromia. In comparing the SS1 and SS2 specimens in this work, the overall scale thicknesses for SS1 were similar to those for SS2, but more spinel was present for SS1.

The composition of the spinel phase was found to vary depending on the steel. Table 4 lists the Cr:Mn and Cr:Fe ratios determined from cross section EDX analysis of the spinel phase for specimens oxidized for 502 h. Table 4 indicates that for the SS1 and SS2 specimens, the ratio of Cr to Mn in the spinel was close to 2:1. However, for SS3, this ratio was closer to 1:1. The SS3 specimens were also found to have significantly more Fe relative to Cr in the spinel than for either the SS1 or SS1 specimens. It has been reported that the presence of Fe can increase the conductivity of the spinel phase [29]. The conductivity of the oxide scale formed on SS3 has been reported to be higher than that for the SS1 specimens. This was attributed to the higher relative amount of Fe present in the spinel on the SS3 specimens [29], but may also be due to higher Mn levels in the spinel. The higher relative amounts of Fe and Mn in the spinel on the SS3 specimens also suggests that the chromia layer may be less protective for this steel, i.e., allowing more Fe and Mn to diffuse through the oxide layer.

4.3. Insulating oxides

Segregation of Si and Al (for SS3) to form insulating oxides at the metal/oxide interface appears to begin in the early stages of oxidation at 800 °C. For SS1 and SS3, evidence of Si segregation to the metal/oxide interface to form SiO_2 after both short and long oxidation times was found by SIMS, XPS and EDX analysis. For SS2, Si segregation to the metal/oxide interface was detected by SIMS; however, it was not detected by either XPS or EDX analysis. This may just be an indication that the silica layer was thinner for SS2. Niobium segregation was also detected by SIMS and XPS for short oxidation times. SS3 contains Al and evidence of Al segregation at the metal/oxide interface, likely in the form of Al_2O_3, was seen after both short and long oxidation times. The formation of both SiO_2 and Al_2O_3 is not surprising since they are thermodynamically more stable than Cr_2O_3 at 800 °C [30]. One problem with the formation of alumina and silica is that both are insulating and thus they increase the electrical resistance of the interconnect [31]. For SS3, this may be especially true since both alumina and silica form. In fact, it is thought that the addition of rare earth elements, such as La, promotes the accumulation of Si at the metal/oxide interface [32]. For SS2, the silica underlayer is not as evident as for SS1; therefore, the conductivity of SS2 oxides may be higher than for SS1. The formation of insulating oxides at the metal/oxide interface may not be entirely detrimental as alumina and silica can both act as a diffusion barrier for other scale-forming elements and improve the adhesion of the oxide scale [31].

4.4. Oxidation process

The general process for oxidation has been previously described and is summarized as follows. First, oxygen from the environment adsorbs on the surface of the metal [22]. Adsorption of oxygen continues until a 2-D layer of adsorbed oxygen completely covers the metal surface [33]. At this point, a thin oxide film rapidly forms on the metal surface [34]. This process is referred to as "transient oxidation", as the film contains oxides of every scale-forming element in the metal in an amount proportional to the amount of the element in the bulk of the metal [3]. The majority of these oxides have a lower thermodynamic stability than the protective oxide [3]. Once a continuous film has formed, the formation of 3-D oxide nuclei occurs at defect sites such as grain boundaries, impurities, dislocations, and surface flaws [22]. These oxide nuclei have the same composition as the protective oxide, which is chromia in this study. Then, the oxide nuclei grow laterally until a continuous protective oxide film covers the surface [22]. The growth of the transient oxides, which are less thermodynamically stable, stops [15]. Some of these oxides will eventually decompose, while others will be incorporated into the outer portion of the protective oxide [15]. Once a continuous film of chromia is formed, the metal that is directly below the oxide film will be depleted in Cr. In order for oxide formation to continue, Cr must be supplied through diffusion from the bulk of the alloy [3]. Subsequent growth of the protective oxide relies on the transport of metal and oxygen ions across

the scale in accordance with parabolic oxidation kinetics [34]. For stainless steels, chromia grows predominantly through the outward diffusion of metal ions, namely Cr^{3+} [10,35]. Typically, the formation of metal ions occurs at the metal/oxide interface, while the formation of oxygen ions occurs at the oxide/gas interface [22].

For the ferritic stainless steels studied in this work, Cr–Mn spinel containing some Fe forms in addition to chromia. The reason for the formation of a separate spinel layer is that Mn has a low solubility in chromia [10]. Spinel formation occurs in the outer portion of the oxide scale because the diffusion of Mn ions through chromia is rapid [36]. The diffusion rates of metal ions through chromia, assuming substitution in cation lattice sites, is as follows: $D_{Mn} > D_{Fe} > D_{Ni} > D_{Cr}$ [37]. Because of this, it is likely that spinel formation occurs predominantly through the reaction of Mn ions with chromia and not through the reaction of Mn and Cr ions with oxygen ions. In the early stages of oxidation, the spinel is not continuous [38].

Through both XPS and SIMS analysis, Mn in its oxidized form was found at the surface of the oxide even after only 15 min of oxidation. When SS1 and SS2 specimens that were oxidized for 15 min, were examined in the SEM, faceted spinel crystals were not clearly visible; however, for the SS3 specimens, many spinel crystals were visible all over the surface of the oxide. For SS1, after 30 min of oxidation, spinel crystals were clearly visible. Therefore, it seems reasonable to assume that at 800 °C, the formation of spinel begins almost immediately.

5. Summary

In this study, the effect of sandblasting and cold rolling on the oxidation behaviour of three ferritic stainless steels, i.e., one with 16–18 wt% Cr (SS1), one with slightly higher Cr and small amounts of Mo and Nb (SS2) and one with 22 wt% Cr plus small amounts of Ni, Al, La and Zr (SS3), in air at 800 °C was studied. The results are summarized as follows:

- Specific mass gain measurements after 502 h of oxidation indicated that the mass gain of SS3 was significantly higher than for either SS1 or SS2, which had similar specific mass gains. For all three steels, the specimens subjected to surface treatment (both cold rolling and sandblasting) had a higher specific mass gain than the as-is specimens.
- For all samples studied, two oxide phases were present in the protective oxide layer: chromia and Cr–Mn spinel. The relative amount of chromia and spinel phases varied with the type of steel. The SS3 specimens had the highest relative amount of spinel, followed by the SS1 specimens and then the SS2 specimens. For SS1 and SS3, surface treatment decreased the relative amount of spinel compared to the as-is specimens. For SS2, all specimens had similar relative amounts of spinel. For SS3, the spinel was enriched in Fe compared to that for either SS1 or SS2.
- The formation of insulating oxides at the metal/oxide interface was observed. For SS1, surface science analysis indicated the formation of SiO_2 at the metal/oxide interface after only 15 min of oxidation at 800 °C. EDX analysis of oxidized cross section specimens after 502 h of oxidation confirmed the presence of this insulating oxide layer at the metal/oxide interface after 502 h of oxidation. For SS2, the presence of SiO_2 and Nb-containing oxides at the metal/oxide interface was detected after 15 min of oxidation; however, Si and Nb segregation were not clearly visible after 502 h of oxidation. For SS3, owing to the presence of both Al and Si in the bulk, the formation of a silica and an underlying alumina layer was noted after both short and long oxidation times. The formation of insulating oxide layers at the metal/oxide interface is not particularly beneficial for SOFC interconnect applications since these oxides further increase the electrical resistance of the interconnect.

Acknowledgements

Funding for this research was provided by the Natural Sciences and Engineering Research Council (NSERC) of Canada and Versa Power Systems (VPS). The assistance of D. Caird (XRD), T. Barker (SEM) and L. Gill (SEM), as well as that of A. He and D. Karpuzov (SIMS and XPS) from the Alberta Centre for Surface Engineering and Science (ACSES) is greatly appreciated.

References

[1] W.Z. Zhu, S.C. Deevi, Mater. Sci. Eng. A 348 (2003) 227–243.
[2] W.J. Quadakkers, H. Greiner, W. Köck, Proceedings of the 1st European SOFC Forum, 1994, pp. 525–541.
[3] C. Ostwald, H.J. Grabke, Corros. Sci. 46 (2004) 1113–1127.
[4] J.M. Rakowski, G.H. Meier, F.S. Pettit, Scripta Mater. 35 (1996) 1417–1422.
[5] H.J. Grabke, E.M. Müller-Lorenz, S. Strauss, E. Pippel, J. Woltersdorf, Oxid. Met. 50 (1998) 241–254.
[6] P.S.N. Stokes, F.H. Stott, G.C. Wood, Mater. Sci. Eng. A 121 (1989) 549–554.
[7] Metal Suppliers Online: Material Property Data, 2006 (http://www.suppliersonline.com).
[8] M.J. Garcia Vargas, L. Lelait, V. Kolarik, H. Fietzek, M. Juez-Lorenzo, Meeting Abstracts: 207th Meeting of The Electrochemcial Society, 2005, p. 244.
[9] L. Cooper, S. Benhaddad, A. Wood, D.G. Ivey, W. Chen, 31st International Cocoa Beach Conference and Exposition on Advanced Ceramics and Composites, Daytona Beach, Florida, January 21–26, 2007, pp. 267–278 (published in Advances in Solid Oxide fuel Cells III).
[10] W.J. Quadakkers, J. Piron-Abellan, V. Shemet, L. Singheiser, Mater. High Temp. 20 (2003) 115–127.
[11] W.F. Smith, in: B.J. Clark, J. Maisel (Eds.), Structure and Properties of Engineering Alloys, second ed., McGraw-Hill, Toronto, 1993, pp. 288–334.
[12] L. Jian, J. Huezo, D.G. Ivey, J. Power Sources 123 (2003) 151–162.
[13] M. Danielewski, R. Filipek, B. Kucharska, Defect Diffus. Forum 137–240 (2005) 965–970.
[14] F.A. Khalid, S.E. Benjamin, Oxid. Met. 54 (2000) 63–71.
[15] S. Leistikow, I. Wolf, H.J. Grabke, Werkst. Korros. 38 (1987) 556–562.
[16] H.J. Grabke, Z. Tökei, C. Ostwald, Steel Res. Int. 75 (2004) 38–46.
[17] M.C. García-Alonso, M.L. Escudero, J.L. González-Carrasco, J. Chao, ISIJ Int. 41 (2001) 56–62.
[18] P. Taylor, R.J. McEachern, D.C. Doern, D.D. Wood, J. Nucl. Mater. 256 (1998) 213–217.
[19] O. Van der Biest, J.M. Harrison, J.F. Norton, Behaviour of High Temperature Alloys in Aggressive Environments: Proceedings of the Petten International Conference, 1979, pp. 681–703.
[20] W.Z. Zhu, S.C. Deevi, Mater. Res. Bull. 38 (2003) 957–972.
[21] S. Leistikow, Behaviour of High Temperature Alloys in Aggressive Environments: Proceedings of the Petten International Conference, 1979, pp. 197–207.
[22] P. Kofstad, High Temperature Corrosion, Elsevier Applied Science, New York, 1998, p. 534.
[23] I. Antepara, I. Villarreal, L.M. Rodríguez-Martínez, N. Lecanda, U. Castro, A. Laresgoiti, J. Power Sources 151 (2005) 103–107.
[24] L.C. De Jonghe, C.P. Jacobson, S.J. Visco, Proceedings of the 6th European Solid Oxide Fuel Cell Forum, vol. 1, 2004, pp. 91–93.
[25] K. Honneger, A. Plas, R. Diethelm, W. Glatz, Solid Oxide Fuel Cells VII: Proceedings of the Seventh International Symposium, vol. 2001-16, 2001, pp. 803–810.
[26] A.V. Virkar, DM England, U.S. Patent No. 6,054,231 (2000).
[27] Q. Wei, M. Eng. Thesis, University of Calgary, Calgary, Alberta, 2004.
[28] D.M. England, Ph.D. Thesis, University of Utah, Salt Lake City, Utah, 2003.
[29] N. Sakai, T. Horita, Y.P. Xiong, K. Yamaji, H. Kishimoto, M.E. Brito, H. Yokokawa, T. Maruyamba, Solid State Ionics 176 (2005) 681–686.
[30] D. Shifler, Corrosion: Fundamentals, Testing, and Protection, ASM International, Materials Park, Ohio, 2003, pp. 650–681.
[31] Z. Yang, J.S. Hardy, M.S. Walker, G. Xia, S.P. Simner, J.W. Stevenson, J. Electrochem. Soc. 151 (2004) A1825–A1831.
[32] F. Riffard, H. Buscail, E. Caudron, R. Cueff, C. Issartel, S. Perrier, Mater. Charact. 49 (2002) 55–65.
[33] S.A. Bradford, Corrosion Control, second ed., CASTI Publishing, Edmonton, Alberta, 2002, 491 pp.
[34] G.E. Wasielewski, R.A. Rapp, in: C.T. Sims, W.C. Hagel (Eds.), The Superalloys, John Wiley and Sons, New York, 1972, pp. 287–316.
[35] P. Kofstad, Solid State Ionics 52 (1992) 69–75.
[36] T. Brylewski, J. Dąbek, K. Przybylski, J. Therm. Anal. Calorim. 77 (2004) 207–216.
[37] H. Kurokawa, K. Kawamura, T. Maruyama, Solid State Ionics 168 (2004) 13–21.
[38] Z. Yang, G. Xia, G.D. Maupin, J.W. Stevenson, J. Electrochem. Soc. 153 (2006) A1852–A1858.